Catal Lett (2012) 142:1286–1294
DOI 10.1007/s10562-012-0904-3

The Role of an Organic Cap in Nanoparticle Catalysis: Reversible Restructuring of Carbonaceous Material Controls Catalytic Activity of Platinum Nanoparticles for Ethylene Hydrogenation and Methanol Oxidation

L. Robert Baker · Griffin Kennedy · James M. Krier · Matthijs Van Spronsen · Robert M. Onorato · Gabor A. Somorjai

Received: 30 July 2012 / Accepted: 6 September 2012 / Published online: 28 September 2012

Abstract Inherent in the colloidal synthesis of nanoparticle catalysts is the presence of an organic capping agent that encapsulates the nanoparticles to prevent aggregation. However, this capping agent often remains present on the nanoparticles during catalytic reaction, and the effect of this coating on catalysis is an important question that will influence the future applications of colloidal nanoparticles. In this study, the structure of poly(vinylpyrrolidone) (PVP) ligands on Pt nanoparticles is probed using sum frequency generation vibrational spectroscopy before and after cap removal by UV light. When the PVP is removed, carbonaceous fragments remain on the surface that dynamically restructure in H_2 and O_2. These fragments form a porous coating around the Pt in H_2 but collapse to a tightly closed shell in O_2. Using ethylene hydrogenation and methanol oxidation as a probe for the catalytic activity of the nanoparticles in H_2 and O_2, respectively, it is shown that the structure of these carbonaceous fragments controls the catalytic activity of the nanoparticles across several orders of magnitude by opening in H_2 and collapsing to block Pt sites in O_2. Kinetic experiments on thermally-cleaned PVP-capped and oleic acid-capped nanoparticles show that these findings apply to multiple capping agents and cleaning methods. This work highlights the dominant role of an organic cap to mediate nanoparticle catalysis and provides one example where capped nanoparticles are dramatically better catalysts than their uncapped analogues.

Keywords Capping agent · Nanoparticles · Nanotechnology · SFG · Microscopy · Spectroscopy and general characterisation · Heterogeneous catalysis · Catalysis

1 Introduction

Traditional methods for catalyst preparation (i.e., incipient wetness and ion exchange) use the reduction of a metal salt inside of a mesoporous oxide [1, 2]. The result is a high surface area catalyst consisting of metal particles with a broad distribution of sizes and morphologies. This type of polydisperse heterogeneous catalyst masks the structure sensitivity inherent in heterogeneous catalysis [3–6] because with this method it is not possible to select nanoparticles of a single size or shape. Recent advances in nanoscience have shown that colloidal synthetic methods can produce monodisperse nanoparticles with well-defined sizes and shapes [7–11]. This advance marked a new era in heterogeneous catalysis where monodisperse nanoparticles serve as model catalysts [12–14] and these catalysts have shown that size and shape control the catalytic activity and selectivity for many reactions [15–21]. These results indicate that colloidal nanoscience is an important tool for the development of new highly selective catalysts necessary to minimize the environmental impact and improve the economic efficiency of numerous commercial chemical processes.

L. R. Baker (✉) · G. Kennedy · J. M. Krier · R. M. Onorato · G. A. Somorjai (✉)
Department of Chemistry, University of California, Berkeley and Chemical and Materials Sciences Divisions, Lawrence Berkeley National Laboratory, Berkeley, CA 94720, USA
e-mail: lrbaker@berkeley.edu

G. A. Somorjai
e-mail: somorjai@berkeley.edu

M. Van Spronsen
Leiden Institute of Chemistry, Leiden University, P.O. Box 9502, 2300 RA Leiden, The Netherlands

In colloidal synthetic methods, nanoparticles are necessarily encapsulated in anorganic polymer or surfactant. This organic coating lowers the surface energy of the nanoparticle to prevent aggregation of the particles [11]; the cap may also help to control the size and shape of the nanoparticles [22]. This gives rise to an important question regarding the effect of the organic cap on the catalytic properties of the nanoparticles. It is traditionally thought that the cap acts as a site blocking agent and lowers the metal surface area available for catalytic reaction [23]. In this light, it has been assumed that colloidal preparation methods are impractical for commercial catalytic applications because the presence of the capping agent decreases the apparent metal dispersion. However, this is an incomplete assumption based on a model that considers the cap as a passive coating rather than a dynamic shell that can adjust under reaction conditions.

It has been observed in the case of Pt–dendrimer complexes that the dendrimer structure, which is highly sensitive to gas/liquid conditions, controls access to the Pt surface [24]. Although the dendrimer blocks the Pt surface in air, it adopts an open structure in water that allows ready access of gasses to the Pt surface. Despite the importance of this effect for nanoparticle catalysis, little effort has been made to directly probe the role of a nanoparticle cap to mediate surface adsorption and catalytic activity. In this work we find that Pt nanoparticles capped with either poly(vinylpyrrolidone) (PVP) or oleic acid (OA) are active for both ethylene hydrogenation and methanol oxidation showing that the organic coating does not prevent nanoparticle catalysis. When the organic coating is removed either by UV light or thermal oxidation, the activity for ethylene hydrogenation increases while the activity for methanol oxidation decreases to almost zero. This surprising result shows that the capped nanoparticles are more active for methanol oxidation than their cleaned analogues.

Because of the high surface energy of metals, it is not possible to maintain a clean metal surface, even under conditions of ultra-high vacuum. With this in mind, it is clear that even catalysts prepared by traditional methods also become "capped" with undefined surface species as these catalysts quickly become contaminated in ambient conditions or during reaction [25]. Accordingly, the capping agent on colloidal nanoparticles represents a well-controlled passivation layer which, as shown here, does not prevent catalysis under reaction conditions. The concept of using an organic coating to increase catalytic activity of a nanoparticle is reminiscent of homogeneous catalysis where ligands are used to tune the activity and selectivity of single metal ions [26], and several examples have already shown that similar effects are also possible on metal clusters [27, 28].

The present work investigates the role of PVP to mediate the catalytic properties of encapsulated Pt nanoparticles. We probe the molecular structure of the PVP cap by sum frequency generations (SFG) vibrational spectroscopy. Ethylene hydrogenation and methanol oxidation then serve as model reactions to probe the catalytic activity in reducing and oxidizing conditions, respectively. Spectral results show that the PVP cap has a strong SFG signal in O_2 atmosphere but disorders in H_2 atmosphere. However, kinetic measurements for ethylene hydrogenation and methanol oxidation show that this capping layer still allows catalysis regardless of the gas conditions. When the PVP is removed by photodecomposition using UV light, carbonaceous fragments remain on the surface that reversibly restructure in H_2 and O_2. In O_2 atmosphere, these carbonaceous fragments form a tightly closed shell around the nanoparticles that blocks catalytic activity, but this shell opens in H_2. As a result, following UV cleaning the nanoparticles are highly active for ethylene hydrogenation but not for methanol oxidation. Kinetic experiments on thermally-cleaned PVP- and OA-capped nanoparticles show similar results indicating that these findings apply to multiple capping agents and cleaning methods. This work highlights the dominant role of an organic coating to mediate nanoparticle catalysis and provides methanol oxidation as one example where capped nanoparticles are dramatically better catalysts than their cleaned analogues.

2 Experimental

2.1 Nanoparticle Synthesis

The Pt nanoparticles were synthesized from chloroplatinic acid hexahydrate and PVP in a 1:4 mass ratio. In a small beaker, 110 mg of chloroplatinic acid was dissolved in 10 mL ethylene glycol. In a separate beaker, 440 mg of PVP was dissolved in 10 mL of ethylene glycol. Once in solution, the two mixtures were combined into a 50 mL two-neck round bottom flask. The solution was purged under vacuum for 15 min. The vessel was then heated to 438 K for 1 h with vigorous mixing under a flow of argon. The resulting nanoparticles were precipitated with acetone and washed three times with ethanol and hexanes. The nanoparticles were then suspended in chloroform. Transmission electron microscopy (TEM) showed that the particles were 4.6 ± 2.8 nm.

To investigate the effect of different capping agents and cleaning methods on reaction kinetics, Pt nanoparticles were synthesized using an alternate method where the capping agent is added after synthesis. This allowed us to add different capping agents to identical nanoparticle aliquots to isolate the cap as the sole variable between two

nanoparticle samples [23]. In a small beaker, 350 mg of chloroplatinic acid was dissolved in 17.5 mL ethylene glycol. In a separate beaker, 350 mg of NaOH was dissolved in 17.5 mL ethylene glycol. Once in solution, the two mixtures were combined in a 50 mL two-neck flask. The solution was purged under vacuum for 15 min. The vessel was then heated to 433 K for 3 h with vigorous mixing under a flow of argon. Aliquots (2 mL) of the resulting nanoparticles were precipitated with 2 M HCl, and then re-dispersed in 2 mL ethanol containing 10 mg of either PVP or OA. TEM showed that the particles were 1.7 ± 0.8 nm.

2.2 Langmuir–Blodgett Deposition

Formation of 2D films of monodisperse nanoparticles to serve as model catalysts is routinely achieved by Langmuir–Blodgett deposition. This technique has been described previously in detail [12, 29]. In short, a suspension of nanoparticles in chloroform is dispersed onto a water surface (18 MΩ). Time is given for the chloroform to evaporate, leaving a 2D dispersion of nanoparticles. The film is then compressed with a mobile barrier, and the surface pressure is monitored as a function of decreasing surface area. The surface pressure corresponds to the density of nanoparticles on the water. When the desired surface pressure is reached, a substrate is pulled out from under the surface of the water, and the film of nanoparticles is deposited onto the substrate. The final density of nanoparticles on the substrate can be controlled by controlling the surface pressure during deposition. A surface pressure of 14 mN/m was used for these studies, and films were deposited using a Nima 611 LB trough. Filter paper served as the surface tension probe.

The substrate used to support the nanoparticles was a TiO_2 thin film (50 nm) deposited on a Si(100) wafer with a thermally grown SiO_2 layer (500 nm). The TiO_2 thin film was deposited on the SiO_2/Si wafer by electron beam evaporation from an oxide source without any substrate heating. Following deposition, the TiO_2 thin film was annealed at 773 K in O_2 to increase crystallinity and ensure a fully oxidized stoichiometry. Analogous samples were prepared for sum frequency generation spectroscopic studies. For these samples, an optically transparent substrate was needed. A sapphire window rather than a Si wafer served as the substrate. A TiO_2 thin film (50 nm) was deposited on the sapphire window by electron beam evaporation, again followed by annealing at 773 K in O_2. The LB technique was then used to deposit a monolayer of the Pt nanoparticles onto the TiO_2 thin films. Electron microscopy showed that the area coverage for Pt on the substrate following LB was 30–50 %.In some cases, TiO_2 used as a Pt support plays an active role in the catalytic chemistry. However, the conclusions reported here are not substrate dependent, and kinetic results have been obtained for identical nanoparticles supported on SiO_2 substrates, and no significant differences were observed.

LB deposition is challenging for OA-capped Pt nanoparticles owing to the high hydrophobicity of the OA. Consequently, for investigating the role of different capping agents, films of the 1.7 nm PVP- and OA-capped nanoparticles were drop cast on a TiO_2 substrate.

2.3 Cap Removal

Immediately prior to reaction, the samples were exposed to UV light in air to remove the PVP capping layer. Two low-pressure mercury (Hg) lamps (Lights Sources Inc., GPH357T5VH/4P) were used as the UV source; the lamps emit at 184 and 254 nm. The two lamps were aligned parallel to each other 2.5 cm apart in a clean Al box. The sample sat 1.2 cm below the lamps. By varying the time of UV exposure, it was possible to control the amount of PVP removed from the Pt nanoparticles. This cleaning is the combined effect of direct photodecomposition of the PVP and oxidation of the PVP by ozone produced from the 184 nm Hg line [30].

X-ray photoelectron spectroscopy (XPS) was used to observe the removal of PVP from the Pt nanoparticles after UV cleaning. Spectra were obtained using a Physical Electronics system (PHI 5400 ESCA/XPS) with an Al anode source. The analyzer was positioned at 50° relative to sample normal. The C1s, N1s, and Pt4f peak areas were normalized by the appropriate sensitivity factors to obtain the surface C:Pt and N:Pt atomic fractions as a function of UV exposure time. Measurements showed that 90 % of the C was removed from the Pt following 3 h UV exposure.

Thermal cleaning in air was used as an alternative to UV cleaning for drop cast samples. For thermal cleaning, the samples were placed in a tube furnace and heated to a desired temperature for 16 h. The PVP- and OA-capped samples were treated at 473 and 573 K, respectively to remove the two capping agents that show different thermal stabilities.

2.4 Sum Frequency Generation Vibrational Spectroscopy

Sum frequency generation (SFG) is a second order, nonlinear process that probes the $X^{(2)}$ tensor. Because $X^{(2)}$ is zero for centrosymmetric media, SFG is only sensitive to a break in inversion symmetry which usually occurs at a surface or interface [31]. Consequently, SFG is useful for obtaining vibrational spectra of surfaces. In this study, SFG is used to obtain the vibrational spectrum of the nanoparticle capping layer in H_2 and O_2 atmospheres.

For SFG experiments, an active/passive mode-locked Nd:YAG laser (Leopard D-20, Continuum) produces 20 ps pulses at a 20 Hz repetition rate. The fundamental output at 1,064 nm was passed through an optical parametric generator/amplifier to generate a tunable infrared (IR) beam (2,700–3,600 cm^{-1}) and a second harmonic visible (VIS) beam (532 nm). The IR (100 μJ) and VIS (100 μJ) beams were spatially and temporally overlapped on the surface of a sapphire window containing the Pt nanoparticles. The VIS and IR beams were incident on the sample at 40° and 50° degrees, respectively, relative to surface normal. The generated SFG signal was then collected and sent to a photomultiplier tube. A gated integrator was used to enhance the signal-to-noise. To collect a spectrum, the IR beam was scanned across the spectral range of interest. All experiments were performed in the ppp polarization combination.

The beams were directed onto the sample using a sapphire prism as shown in Fig. 1. A solution of deuterated polystyrene (d8) in deuterated decalin (d18) served as an index matching liquid between the prism and substrate that did not interfere with transmission of the IR beam at the C–H stretch frequency. The catalyst surface was pressed into thermal contact with an aluminum heating block to heat the catalyst to the desired temperature. A recess in the heating block allowed for the flow of gasses across the catalyst surface. A metal bellows circulation pump provided gas mixing. A gas tight seal was made between the sapphire window and the heating block using a Kalrez O-ring.

2.5 Kinetic Measurements

A stainless steel batch mode reactor was used to determine the reaction rates for ethylene hydrogenation and methanol oxidation on the Pt nanoparticle catalysts before and after UV cleaning. The catalyst temperature was controlled with a boron nitride substrate heater. A metal bellows circulation pump provided gas mixing. For ethylene hydrogenation, gas pressures were 10 Torr ethylene, 100 Torr H_2, and 650 Torr He, and the catalyst temperature was 298 K. For methanol oxidation, gas pressures were 10 Torr methanol, 50 Torr O_2, and 700 Torr He, and the catalyst temperature was 333 K. The methanol was purified by freeze-pump-thawing cycles. Each catalyst was tested for 2 h, and reaction products were monitored as a function of time using a gas chromatograph with a thermal conductivity detector. Rates for ethylene hydrogenation and methanol oxidation were measured on each catalyst before and after cleaning.

3 Results and Discussion

Figure 2a shows the SFG spectra of PVP-capped Pt nanoparticles in sequential gas environments. As the gas environment is initially cycled between H_2 and O_2, the SFG signal is higher in O_2 and decreases in H_2 corresponding to a structural reconfiguration of PVP on the Pt, and this effect has been discussed previously [32]. In summary, because of selection rules, SFG is sensitive not only to the individual molecular susceptibilities, but also to the net susceptibility of the entire ensemble of molecules at an interface. This net susceptibility depends strongly on the relative orientation of molecules at the interface. It is usually assumed that systems showing greater SFG signal intensity have a more highly ordered interface than those showing weaker intensity because a net disorder leads to canceling out of signal from individual molecular oscillators. Accordingly, we assign the loss of signal intensity going from O_2 to H_2 atmosphere as H_2-induced disordering of the PVP. However, after the first H_2/O_2 cycle, the PVP settles into a relatively stable configuration on the Pt, and minimal restructuring occurs as the gas environment continues to change between reducing and oxidizing conditions.

This is in strong contrast to spectra shown on identical nanoparticles following UV cleaning to remove PVP from the Pt surface. Figure 2b shows the raw spectra of UV-cleaned nanoparticles first in H_2 then in O_2. The spectrum obtained in H_2 shows a much higher nonresonant intensity with resonant features appearing as negative peaks against the high background. This effect, which is common in

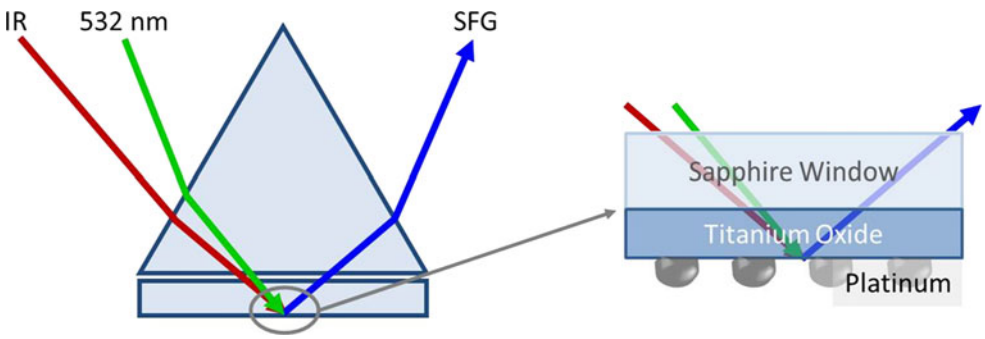

Fig. 1 Diagram showing how a sapphire prism directed the VIS and IR beams onto the catalyst surface for SFG vibrational spectroscopy. The catalyst was prepared on the *back side* of a sapphire window and consisted of a thin film of TiO_2 acting as a support for Pt nanoparticles

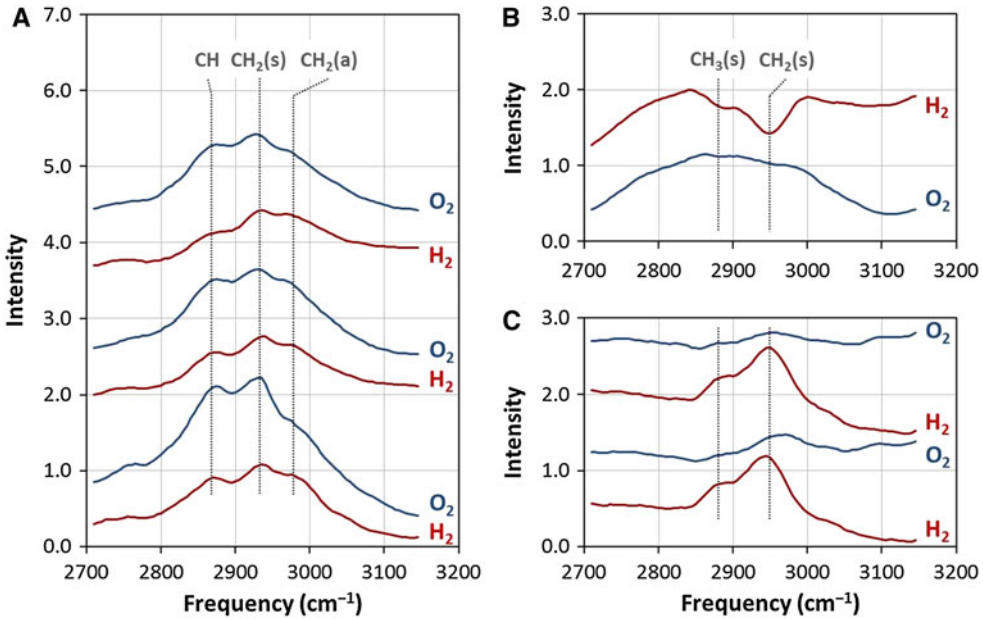

Fig. 2 SFG spectra of the PVP-capped Pt nanoparticles before UV cleaning (**a**) and after UV cleaning for 10 min (**b** and **c**). Spectra were obtained in 100 Torr of H_2 or O_2 in a background of Ar at 60 °C. A *boxcar* average over 5 data points improved signal-to-noise. In **a** and **c** the spectra are arbitrarily offset for clarity and were obtained sequentially from *bottom* to *top*. **b** Shows the raw spectra with no offset of UV-cleaned nanoparticles first in H_2 then in O_2. The spectrum obtained in H_2 shows a much higher nonresonant intensity with resonant features appearing as dips in the high background. This is a result of the phase mismatch between the resonant and nonresonant contributions of the spectrum. By subtracting the raw spectra from a *baseline* obtained in Ar, the negative features are inverted to appear positive for clarity (shown in **c**). Analysis of the resonant features in these spectra shows that before UV cleaning the PVP has a conformation that does not significantly change depending on the gas environment. However, following UV cleaning, carbonaceous fragments are found on the surface that are dynamic and reversibly restructure in H_2 and O_2

SFG, is a result of the phase mismatch between the resonant and nonresonant contributions of the spectrum. By subtracting the raw spectra from a baseline obtained in Ar, the negative features are inverted to appear positive for clarity (see Fig. 2c). The enhanced nonresonant signal of the UV-cleaned catalyst is a result of H spillover from the Pt resulting in a reduced TiO_2 support, and the effect is completely reversible in O_2. In the PVP-capped sample, the nonresonant contribution to the spectrum is low even in H_2 because the PVP blocks H spillover to the TiO_2.

Figure 2c shows that after UV cleaning as the atmosphere is cycled between H_2 and O_2, carbonaceous fragments are present on the Pt surface, and these fragments reversibly restructure, adopting a structure that is strongly SFG active in H_2, and a structure which is almost entirely SFG inactive in O_2. It may be tempting to conclude that O_2 reacts with the remaining cap on the Pt surface to catalyze its complete removal. However, this is not the case as can be seen by the reversible appearance of the molecular vibrations when H_2 is re-introduced to the system. This change occurs reversibly over multiple cycles with no sign of signal decrease over time that would suggest eventual removal of the carbonaceous fragments.

It is also evident that the vibrational modes observed following UV cleaning are not the same as those observed from the intact PVP cap. Initially the vibrational modes observed on PVP-capped Pt (see Fig. 2a) match closely the assignments previously reported by infrared and Raman for PVP–Pt complexes [33]. Following UV cleaning, the peaks observed are attributable to CH_2 and CH_3 symmetric stretching modes outside of a 5-membered ring. It is also important to note that XPS measurements indicate that the surface C has decreased more than 85 % compared to the fully-capped nanoparticles following UV cleaning. It is not definitive whether the carbonaceous fragments observed by SFG after cleaning are photodecomposition products of PVP, or if they represent contamination of the UV-cleaned Pt surface, which would be unavoidable in ambient. However, it is clear that additional UV cleaning does little to remove these species.

Figure 3 shows the catalytic activity of the Pt nanoparticles for ethylene hydrogenation and for methanol oxidation before and after UV cleaning. We selected these two reactions because they operate at low temperature (i.e., 298 and 333 K, respectively) and allowed us to observe the effects of the cap structure on the catalytic activity of the nanoparticles in H_2 and O_2 atmospheres. The PVP-capped Pt nanoparticles are active for both reactions as shown in Fig. 3a, b. However, following UV cleaning, the activity of the nanoparticles for ethylene hydrogenation and methanol

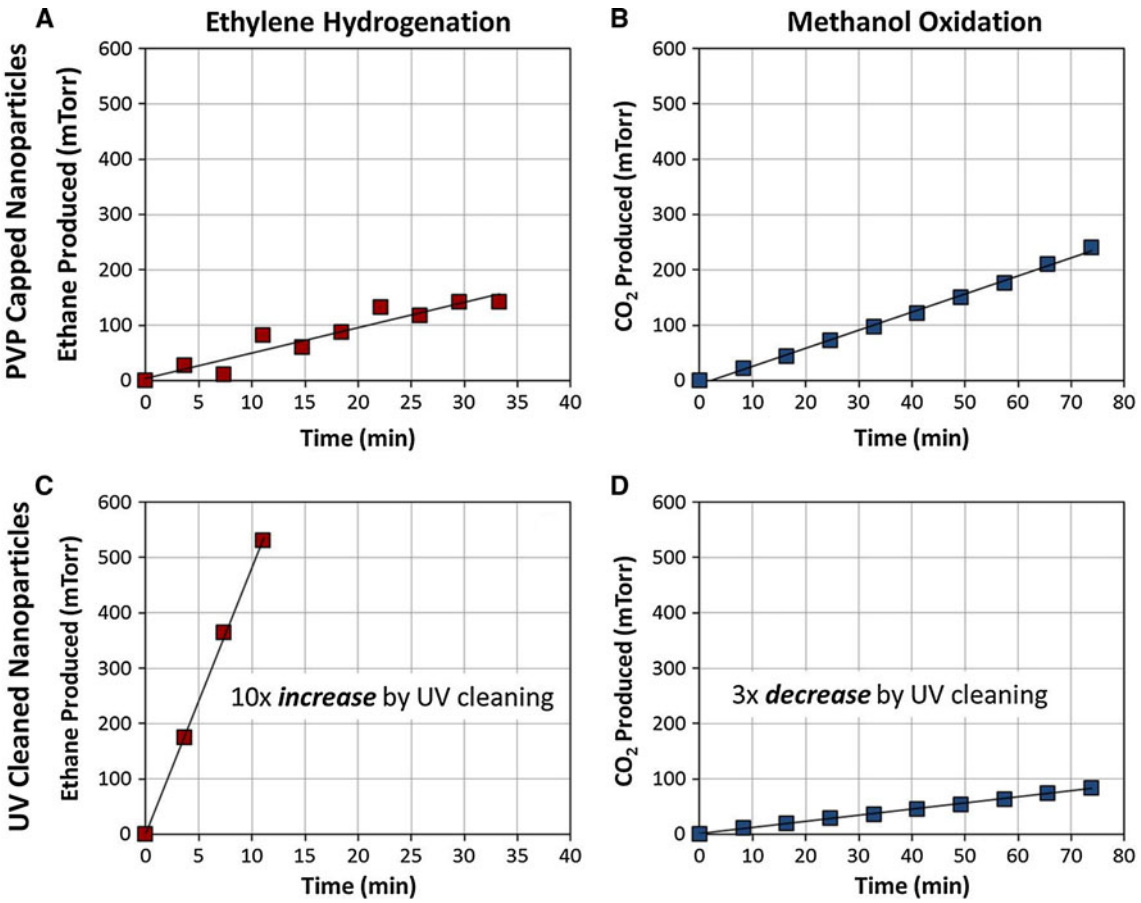

Fig. 3 Formation of reaction products as a function of time on the Pt nanoparticles for ethylene hydrogenation and methanol oxidation before UV cleaning (**a**, **b**) and after UV cleaning for 10 min (**c**, **d**). These results show that UV cleaning has a diverging effect on the rates of ethylene hydrogenation which increases by a factor of *10* and methanol oxidation which decreases by a factor of *3*. Only CO_2 production is shown for methanol oxidation. However, formaldehyde was also produced as a minor product before and after UV cleaning

oxidation diverge. Figure 3c, d show that following UV cleaning, the rate of ethylene hydrogenation increases by a factor of 10 while the rate of methanol oxidation decreases by a factor of 3. This represents a 30-fold divergence on the effect of UV cleaning for these two reactions. We note that formaldehyde is also formed at $\sim$30 % selectivity during methanol oxidation. Formaldehyde production is not shown in Fig. 3 because it follows the same trend as CO_2.

Figure 4 shows the activity of the catalyst following UV cleaning where the catalyst is cycled several times between ethylene hydrogenation and methanol oxidation. The rates are normalized to the initial rate for each reaction prior to UV cleaning. It can be seen that the rates for both ethylene hydrogenation and methanol oxidation are reversibly affected by the removal of the PVP cap. It is clear from previous studies that the thermal stability of the nanoparticles decreases following cap removal, so the UV-cleaned nanoparticles agglomerate during reaction [32]. Nanoparticle agglomeration results in a loss of Pt surface sites which would lead to a decrease in catalyst activity. However, the ethylene hydrogenation kinetics show that the removal of PVP more than compensates for nanoparticle agglomeration resulting in a tenfold net increase in the reaction rate. Consequently, the loss of activity for methanol oxidation following UV cleaning cannot simply be a result of nanoparticle agglomeration which would not be reversible between reactions.

In the case of ethylene hydrogenation, the increase in catalyst activity after cleaning is easily understood based on the increased number of Pt sites available following PVP removal. In the case of methanol oxidation, it is surprising that cap removal would have a negative effect on the catalytic activity. It appears that the structure of the carbonaceous fragments observed on the Pt following UV cleaning controls the catalytic properties of the uncapped nanoparticles. We suggest that these carbonaceous fragments which do little to prevent access to the Pt in H_2 atmosphere, collapse to a tightly closed shell around the Pt in O_2 atmosphere.

To confirm this model in which carbonaceous fragments form a porous coating around the Pt in H_2 but collapse to a

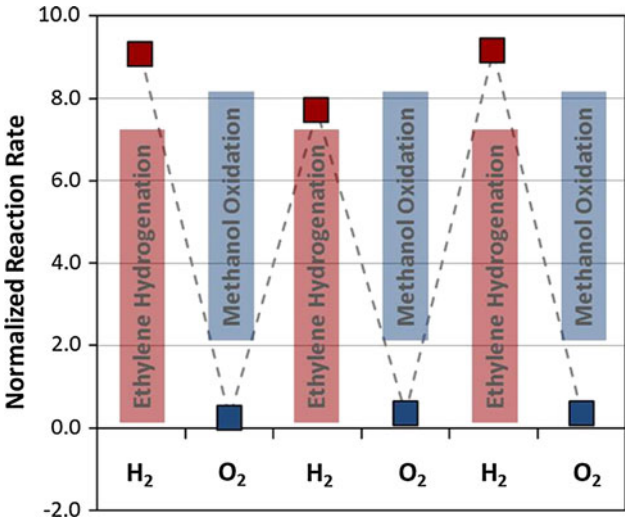

Fig. 4 The reaction rates for ethylene hydrogenation and methanol oxidation on a single catalyst following UV cleaning for 10 min. The reaction rates are normalized to the initial rate for each reaction before UV cleaning. The results show that the diverging effect of UV cleaning on the two reactions is reversible and appears to correlate with the restructuring of carbonaceous fragments on the Pt surface observed by SFG

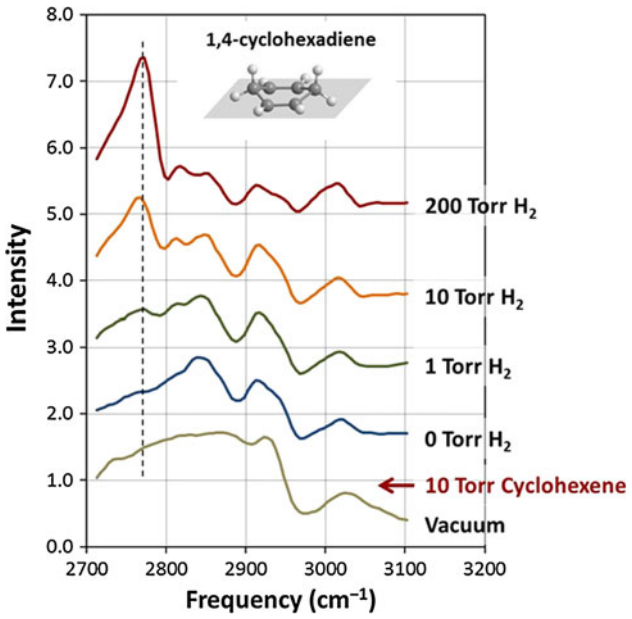

Fig. 5 SFG spectra of 10 Torr cyclohexene in increasing H_2 pressure on Pt nanoparticles after UV cleaning for 60 min. In this experiment, the nanoparticles are supported directly on a SiO_2 prism. Cyclohexene dehydrogenates on Pt to form a 1,4-cyclohexadiene surface intermediate that is characterized by a strong feature in the SFG spectrum at 2,760 cm^{-1}. This feature is known to form on an atomically clean Pt surface even in the absence of H_2. In this case, the feature is initially absent from the spectrum, but grows in with increasing H_2 pressure. This indicates that H_2 is needed to open the carbonaceous shell on the UV-cleaned Pt nanoparticles and allow cyclohexene to access the Pt

tightly closed shell in O_2, we used cyclohexene to probe the accessibility of reactants to the Pt surface. Cyclohexene forms a 1,4-cyclohexadiene surface intermediate on Pt [34]. This is a dehydrogenation product of the cyclohexene and forms even in the absence of H_2. The 1,4-cyclohexadiene species has a distinct molecular vibration at 2,760 cm^{-1} which is spectrally well resolved from any resonant modes of the capping agent. Consequently, cyclohexene represents a suitable probe molecule. To avoid changes in the nonresonant background with changing H_2 pressure, this experiment was performed using Pt nanoparticles supported directly on an SiO_2 prism. Figure 5 shows the results of this experiment. When cyclohexene is introduced in the gas phase to UV-cleaned Pt nanoparticles, no 1,4-cyclohexadiene is observed in the SFG spectrum. Only weak features at 2,840 and 2,910 cm^{-1} appear which we attribute to physisorbed cyclohexene. However, as the H_2 pressure is increased from 0 to 200 Torr, a strong feature at 2,760 cm^{-1} grows in corresponding to 1,4-cyclohexadiene. Because this feature forms on an atomically clean Pt single crystal surface even in the absence of H_2 [34] we conclude that for the UV-cleaned nanoparticles H_2 is needed to open the carbonaceous shell and allow cyclohexene to access the Pt. It is important to note that in this experiment the nanoparticles were pre-reduced with H_2, so that the oxidation state of Pt is not changing during the experiment.

Figure 6a shows the effect of UV cleaning time on the activity of the Pt nanoparticles for ethylene hydrogenation and methanol oxidation. The activity for each reaction is normalized to the initial activity of the PVP-capped nanoparticles before UV cleaning. For ethylene hydrogenation the rate increases with increased cleaning time, while for methanol oxidation the rate decreases with increased cleaning time. Following 3 h there is a 200-fold divergence of the rates for these two reactions. This suggests that with increased cleaning, the carbonaceous shell on the Pt nanoparticles becomes tighter and tighter in O_2; however, it can continue to open in H_2 allowing access to the Pt. In fact, the ethylene hydrogenation rate after UV cleaning is slightly greater than expected based on the geometric surface area of the Pt as determined by TEM. This suggests that the carbonaceous fragments have almost no site blocking effect in H_2. Figure 6b shows the corresponding C and N surface concentrations as a function of UV cleaning time measured by XPS. After 30 min, the concentration of N is below the limit of detection by XPS. The C concentration also levels off after 30 min to a steady value representing only 10 % of the initial C. Again it is impossible to distinguish if this C is a decomposition product of the PVP or if it is contamination of the cleaned Pt surface.

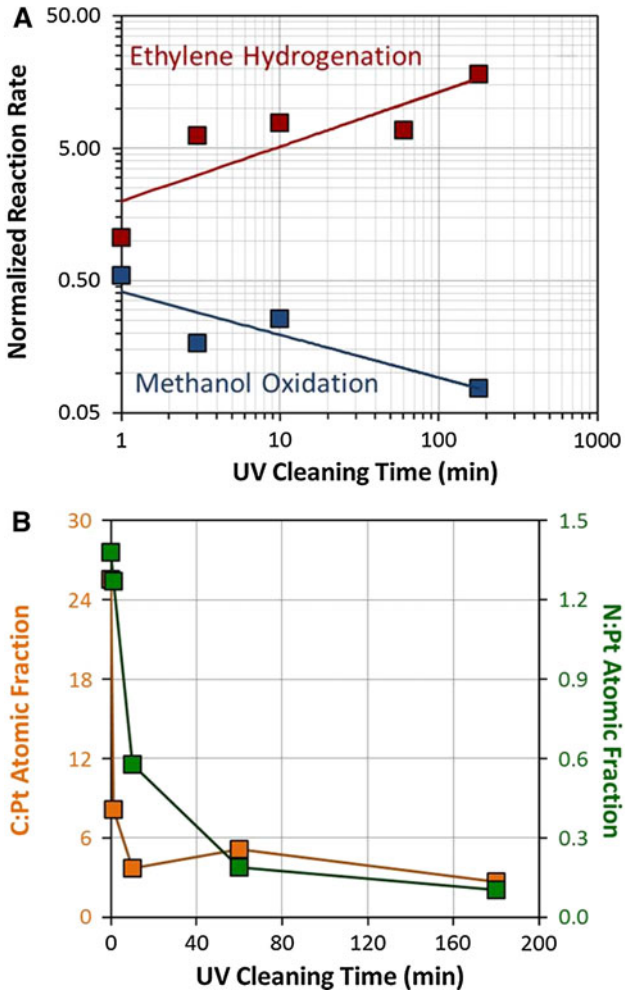

Fig. 6 **a** Reaction rates as a function of UV cleaning time for ethylene hydrogenation and methanol oxidation. The reaction rates are normalized to the initial rate for each reaction before UV cleaning. The results show that the rates of the two reactions continue to diverge with increased cleaning time, eventually showing a 200-fold difference in activity. **b** C:Pt and N:Pt atomic fractions measured by XPS as a function of UV cleaning time. The N concentration on the surface drops below the limit of detection after 30 min of UV cleaning. The C concentration on the surface also levels off at a value representing only 10 % of the initial C from the PVP capping layer

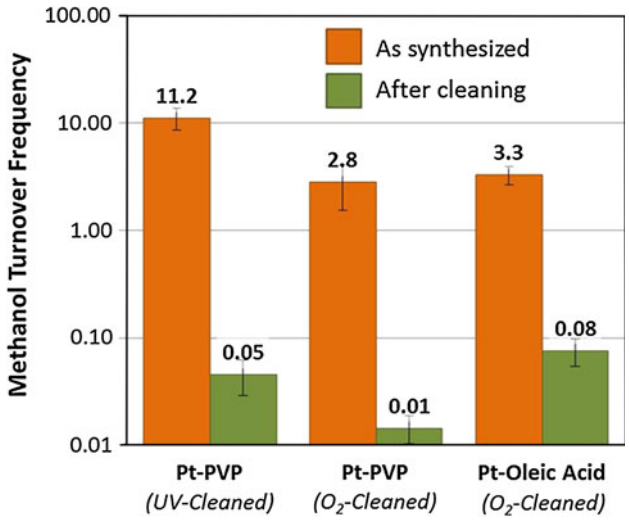

Fig. 7 Methanol oxidation turnover frequency (TOF) for Pt nanoparticle catalysts before and after cap removal. TOF is given as the number of methanol molecules converted per Pt site per s. The number of platinum sites was determined from the measured rate of ethylene hydrogenation using a known TOF. Consequently, *each bar* shows the methanol oxidation rate relative to the ethylene hydrogenation rate on the same catalyst. Data is shown for all three types of nanoparticles studied (i.e., UV-cleaned Pt–PVP, thermally-cleaned Pt–PVP, and thermally-cleaned Pt–OA). Noting that this graph is on a log-scale, the Pt activity for methanol oxidation is shown to decrease for each catalyst by a factor of between 50 and 250 following cap removal

To determine if the formation of this carbonaceous shell is a general phenomenon, we synthesized Pt nanoparticles using an alternate method where the capping agent is added after synthesis. This allowed us to add different capping agents to identical nanoparticle aliquots to isolate the cap as the sole variable between two nanoparticle samples. For this experiment, PVP and OA were used as capping agents in two separate aliquots, and the activity of these catalysts were monitored for ethylene hydrogenation and methanol oxidation before and after cleaning. In this case, thermal oxidation in a tube furnace was used for cap removal rather than UV cleaning. The OA-capped nanoparticles were cleaned at 473 K, and the PVP-capped nanoparticles were cleaned at 573 K. This temperature for PVP removal is consistent with previous work on the thermal degradation of Pt–PVP complexes [33]. Following cleaning the PVP- and OA-capped nanoparticles showed a 100-fold and 30-fold increased activity for ethylene hydrogenation, respectively.

Figure 7 shows the effect of cap removal on the activity for methanol oxidation. In this figure, the methanol oxidation rate for each catalyst is represented as a turnover frequency normalized to the number of Pt active sites determined by ethylene hydrogenation [23]. Consequently, each bar shows the methanol oxidation rate relative to the ethylene hydrogenation rate on the same catalyst. Data is shown for all three types of nanoparticles studied (i.e., UV-cleaned Pt–PVP, thermally-cleaned Pt–PVP, and thermally-cleaned Pt–OA). Noting that this graph is on a log-scale, the Pt activity for methanol oxidation is shown to decrease for each catalyst by a factor of between 50 and 250 following cap removal. Because these values are normalized to the catalyst activity for ethylene hydrogenation, this cannot be the result of nanoparticle agglomeration. It seems clear that for methanol oxidation, the capped nanoparticles are dramatically more active than their cleaned analogues, and this finding applies to multiple capping agents and cleaning methods.

4 Conclusions

We studied the catalytic activity of PVP- and OA-capped Pt nanoparticles for ethylene hydrogenation and methanol oxidation before and after cap removal. We find that the capped nanoparticles are active for both reactions showing that the organic coating does not prevent nanoparticle catalysis. However, the cleaned nanoparticles are only active for ethylene hydrogenation. The rate of ethylene hydrogenation is substantially higher on the cleaned particles relative to the capped particles, but the rate of methanol oxidation decreases to nearly zero following cap removal either by UV light or by thermal oxidation.

SFG shows that, following cleaning treatments, carbonaceous fragments are still present on the nanoparticles. These carbonaceous fragments are dynamic and reversibly restructure in alternating H_2 and O_2 atmospheres. It appears that a carbonaceous shell forms on the uncapped Pt nanoparticles that is tightly closed in O_2 but becomes permeable in H_2. Using cyclohexene as a probe molecule, we show that following UV cleaning, reactant molecules can only access the Pt when H_2 is present to open the carbonaceous shell.

These results demonstrate the important role of an organic cap to mediate the catalytic properties of nanoparticles. We find that the presence of an organic cap does not prevent catalysis. In fact, for methanol oxidation the capped nanoparticles are more than 10 times more active than their cleaned analogues. Accordingly, the capping agent on colloidal nanoparticles represents a well-controlled passivation layer which does not prevent catalysis under reaction conditions. That this coating may improve catalytic performance for certain reactions argues that the capping agent is a dynamic component of the active catalyst which consists of both a metal nanoparticle and an organic coating.

Acknowledgments This work was funded by the Helios Solar Energy Research Center and by the Chemical and Materials Sciences Divisions, which are supported by the Director, Office of Science, Office of Basic Energy Sciences of the U.S. Department of Energy under Contract No. DE-AC02-05CH11231.

References

1. Ertl G, Knozinger H, Weitkamp J (eds) (1999) Preparation of solid catalysts. Wiley, Weinheim
2. Tsoncheva T, Dal Santo V, Gallo A, Scotti N, Dimitrov M, Kovacheva D (2011) Appl Catal A Gen 406:13
3. Strongin DR, Carrazza J, Bare SR, Somorjai GA (1987) J Catal 103:213
4. McCrea KR, Parker JS, Somorjai GA (2002) J Phys Chem B 106:10854
5. Andersson MP, Abild-Pedersen E, Remediakis IN, Bligaard T, Jones G, Engbwk J, Lytken O, Horch S, Nielsen JH, Sehested J, Rostrup-Nielsen JR, Norskov JK, Chorkendorff I (2008) J Catal 255:6
6. Kliewer CJ, Bieri M, Somorjai GA (2009) J Am Chem Soc 131:9958
7. Ahmadi TS, Wang ZL, Green TC, Henglein A, El-Sayed MA (1924) Science 1996:272
8. Peng X, Wickham J, Alivisatos AP (1998) J Am Chem Soc 120:5343
9. Puntes VF, Krishnan KM, Alivisatos AP (2001) Science 291:2115
10. Oh M, Mirkin CA (2005) Nature 438:651
11. Yin Y, Alivisatos AP (2005) Nature 437:664
12. Song H, Kim F, Connor S, Somorjai GA, Yang P (2004) J Phys Chem B 109:188
13. Rioux RM, Song H, Hoefelmeyer JD, Yang P, Somorjai GA (2004) J Phys Chem B 109:2192
14. Song H, Rioux RM, Hoefelmeyer JD, Komor R, Niesz K, Grass M, Yang P, Somorjai GA (2006) J Am Chem Soc 128:3027
15. Bratlie KM, Lee H, Komvopoulos K, Yang P, Somorjai GA (2007) Nano Lett 7:3097
16. Kuhn JN, Huang W, Tsung C-K, Zhang Y, Somorjai GA (2008) J Am Chem Soc 130:14026
17. Grass M, Rioux R, Somorjai G (2009) Catal Lett 128:1
18. Grass ME, Joo SH, Zhang Y, Somorjai GA (2009) J Phys Chem C 113:8616
19. Kliewer CJ, Aliaga C, Bieri M, Huang W, Tsung C-K, Wood JB, Komvopoulos K, Somorjai GA (2010) J Am Chem Soc 132:13088
20. Witham CA, Huang W, Tsung C-K, Kuhn JN, Somorjai GA, Toste FD (2010) Nat Chem 2:36
21. Alayoglu S, Aliaga C, Sprung C, Somorjai G (2011) Catal Lett 141:914
22. Zhang Y, Grass ME, Kuhn JN, Tao F, Habas SE, Huang W, Yang P, Somorjai GA (2008) J Am Chem Soc 130:5868
23. Kuhn JN, Tsung C-K, Huang W, Somorjai GA (2009) J Catal 265:209
24. Albiter MA, Crooks RM, Zaera F (2009) J Phys Chem Lett 1:38
25. Lu J, Fu B, Kung MC, Xiao G, Elam JW, Kung HH, Stair PC (2012) Science 335:1205
26. Gorin DJ, Sherry BD, Toste FD (2008) Chem Rev 108:3351
27. Li Y, Liu JH-C, Witham CA, Huang W, Marcus MA, Fakra SC, Alayoglu P, Zhu Z, Thompson CM, Arjun A, Lee K, Gross E, Toste FD, Somorjai GA (2011) J Am Chem Soc 133:13527
28. Mitsudome T, Mikami Y, Matoba M, Mizugaki T, Jitsukawa K, Kaneda K (2012) Angew Chem Int Ed 51:136
29. Bratlie KM, Komvopoulos K, Somorjai GA (2008) J Phys Chem C 112:11865
30. Aliaga C, Park JY, Yamada Y, Lee HS, Tsung C-K, Yang P, Somorjai GA (2009) J Phys Chem C 113:6150
31. Shen YR (2003) The principles of nonlinear optics. Wiley-Interscience, Hoboken
32. Krier JM, Michalak WD, Baker LR, An K, Komvopoulos K, Somorjai GA (2012) J Phys Chem C 116:17540
33. Borodko Y, Habas SE, Koebel M, Yang P, Frei H, Somorjai GA (2006) J Phys Chem B 110:23052
34. Yang M, Chou KC, Somorjai GA (2003) J Phys Chem B 107:5267